Reliability Engineering and System Safety 267 (2026) 111817

Contents lists available at ScienceDirect

Reliability Engineering and System Safety

journal homepage: www.elsevier.com/locate/ress

An analytical method for reliability and resilience evaluation of power distribution systems with mobile power sources

Gengfeng Li *, Dingmao Zhang, Zhaohong Bie

State Key Laboratory of Electrical Insulation and Power Equipment, School of Electrical Engineering, Xi'an Jiaotong University, Xi'an 710049, China

A R T I C L E I N F O

Keywords:
Reliability evaluation
Resilience evaluation
Analytical method
Distribution system
Mobile power source

A B S T R A C T

With the gradual expansion of distribution system scales, increasing structural complexity, and growing uncertainties caused by the integration of mobile power sources (MPSs) and various renewable energy sources, higher demands are placed on distribution system reliability and resilience evaluation. This paper proposes an analytical method for reliability and resilience evaluation of distribution systems with MPS, based on the probability expectation and probability density evolution. First, a modeling approach for MPS is presented, and the evaluation is divided into long-term reliability evaluation and short-term resilience evaluation according to the evaluation timescale and the level of system disruption risk. Next, the backup power supply strategy of MPS for failure nodes is investigated in the context of reliability and resilience evaluations. Subsequently, an analytical method for evaluating the reliability and resilience of distribution systems with MPS is proposed based on probability theory and probability density evolution. Additionally, reliability and resilience indices and their calculation methods are introduced. The effectiveness and efficiency of the proposed method are validated through case studies on the modified IEEE 123-node system.

1. Introduction

The distribution system is a critical link connecting the transmission system and the consumer system, and the end is connected to the load, which is directly related to the continuity and reliability of power supply to the consumers [1]. According to statistics, more than 80 % of customer power outages are related to distribution system failures [2–4]. With the development of power systems, the size and complexity of distribution systems have gradually increased, and the requirements for system reliability have risen [5,6]. In addition, the frequent occurrence of high-impact and low-probability (HILP) natural disasters in recent years has caused damage to the distribution system, resulting in economic losses to the society due to power outages of consumers [7,8]. MPSs are increasingly being used in distribution systems nowadays due to their flexibility as a backup power source to improve the reliability and resilience of the distribution system [9,10]. It is therefore essential to evaluate the reliability and resilience of distribution systems containing MPSs to guide the planning and operation of the system.

MPSs include truck-mounted mobile emergency generators (MEGs) [11], and mobile energy storage systems (MESSs) [12,13], which are capable of continuing to supply power to the nodes as a back-up power source after a system failure. Several studies have been conducted around the selection of MPS stations, routing and scheduling strategies of MPSs. Reference [14] consider energy storage (ES) system cost minimization, enhancement of electric vehicle resilience, and peak load reduction to determine the optimal sizing of ES for a fast electric vehicle charging station. Stochastic power flow is used to establish an effective optimization model for site and size planning of electric vehicle charging station [15]. Before the HILP event, MPSs are pre-deployed in the distribution system to enable rapid pre-restoration, thereby enhance the survivability of power supply to critical loads [16]. After the events, MPSs are dynamically dispatched according to the restoration [17]. Co-optimized scheduling of MPS and repair crews can better improve the resilience level of the system [18,19]. Reference [20] considers the combination of the distribution system and transportation in dispatching MPSs. These studies address the scheduling strategies of MPSs in pre-disaster and in-disaster situations, and confirm that MPSs can effectively improve the reliability and resilience level of the system. However, there are still fewer studies that evaluate the reliability and resilience of distribution systems containing MPSs.

Existing methods for evaluating the reliability and resilience of distribution systems containing MPSs mainly use simulation method,

* Corresponding author.
E-mail address: gengfengli@mail.xjtu.edu.cn (G. Li).

https://doi.org/10.1016/j.ress.2025.111817
Received 14 January 2025; Received in revised form 16 July 2025; Accepted 24 October 2025
Available online 26 October 2025

where evaluation results are obtained through sampling of component states, analysis of system scenarios, and statistical analysis [21,22]. A sequential Monte Carlo method is used to evaluate the reliability of microgrids with local and mobile generation and intraday reconfiguration [23]. Reference [24] extends evaluation of reliability of the distribution system including vehicle-to-home and vehicle-to-grid using quadratic optimization, optimal power flow and sequential Monte Carlo methods. A resilience quantification framework for active distribution system with mobile energy storage and four resilience evaluation indices are developed and measured in simulation [25]. The simulation method has the advantages of simple algorithms and application to complex scenarios, but the computational efficiency becomes lower as uncertainty in the system increases. In resilience evaluation, the optimization has to be solved to obtain the repair strategy for each sampled scenario, slowing down the efficiency of the evaluation. In addition, when the system contains MPSs, the system uncertainty increases, the system indices are harder to converge, more scenarios need to be sampled, and the evaluation takes longer time. To provide guidance on distribution system operation in real time, it is crucial to improve the computational efficiency of distribution system reliability and resilience evaluation.

Analytical methods calculate reliability and resilience indices by analyzing the probabilities and impact consequences of various anticipated events. The analytical method can avoid the need for a large number of samples and the computational burden of solving optimization problems in resilience evaluation. Compared to the simulation method, the analytical method is more computationally efficient and has clear mathematical and physical concepts [26–28]. Reference [29] proposes a distribution system resilience evaluation analytical approach based on instantaneous availability increments and probability density evolution methods, improving the evaluation efficiency. An analytic approach based on Markov models is applied to evaluate the reliability of distribution system with the penetrations of mobile energy storage system and intermittent distribution sources [30]. Reference [31] defines the resilience evaluation of distribution systems as a multi-criteria decision problem and the resilience is quantified using graph theory and Choquet integrals. In [32], the resilience index-related probability events are established through the utilization of energization paths, with the probabilistic resilience index being explicitly defined employing the total probability theorem, the conditional probability formula, and an energization-path-topology simplification approach. However, the uncertainty of MPSs and the randomness of multiple component failures under extreme events bring challenges to the application of the analytical method. These studies are insufficient for modeling the operating modes of MPS in distribution systems by analytical methods, so it is necessary to propose a computationally efficient and accurate method for reliability and resilience evaluation of distribution systems considering MPSs.

Therefore, this paper proposes an efficient and accurate analytical method for reliability and resilience evaluation of distribution systems containing MPSs using probabilistic expectation and probability density evolution methods. First, the reliability model of MPS is established, and the evaluations is divided into long-term reliability evaluation and short-term resilience evaluation based on the time scale and the risk of disruption to the system. Next, the long-term reliability evaluation process is proposed, and the reliability evaluation index system and calculation method are presented. Then, the short-term resilience evaluation process is proposed, considering the ex-ante deployment and in-ante scheduling strategy of MPS, and the resilience evaluation index system and calculation method are introduced. Finally, the effectiveness and efficiency of the proposed method are validated through case studies on the modified IEEE 123-node system. In summary, the main contributions and innovations of this paper are as follows:

(1) An analytical evaluation framework is proposed for assessing the reliability and resilience of distribution systems with MPSs, using probabilistic expectation and probability density evolution. This framework overcomes the limitations of simulation-based approaches and enhances evaluation efficiency.
(2) A detailed reliability model of MPSs is developed, explicitly incorporating the outage time of a failure node using MPS backup power, and distinguishing between MEGs and MESSs to improve modeling precision.
(3) A MPS dispatch strategy is introduced, guided by node and zone importance metrics, enabling effective pre-deployment and post-disaster transfer to enhance system resilience.
(4) The method is validated on the modified IEEE 123-node system, achieving comparable accuracy to simulation methods, with less than 0.5 % error in reliability and less than 0.1 % error in resilience evaluation, while reducing computation time by approximately 1400 times and 60 times, respectively.

This paper is organized as follows. Section 2 describes the MPS reliability model and scenarios for reliability and resilience evaluation of distribution systems containing MPSs. In Section 3, the long-term reliability evaluation method is presented. Section 4 proposes the method of short-term resilience evaluation. Section 5 reports and analyses the numerical results and the conclusion is provided in Section 6.

2. MPS reliability modeling

This section introduces the application of MPS in distribution systems, modelling method, and categorizes scenarios for evaluating distribution systems containing MPS, providing a foundation for reliability and resilience evaluation.

2.1. MPS Backup Power Strategy

The MPS includes MPG and MESS, which is utilized as a backup power source to continue powering the failure node, and its power supply strategy is shown in Fig. 1. An example of a MESS is given, in which it is assumed that the power and capacity of the MESS is sufficient. When line failure occurs in the system, the MESS is dispatched according to the importance of the failure nodes, while the repair crew is dispatched to repair the failure. Once the failure line repair is complete, the MESS will be transferred and dispatched until power is restored to all failure nodes.

For nodes with MPS backup power supply, the time from line failure to the time the MPS is backed up is the outage time t_o, which includes waiting time t_w, traffic time t_{ra}, and installation time t_i. Waiting time t_w refers to the time when the number or power of MPS is not enough to supply power to all the failure nodes at the same time, the nodes ranked

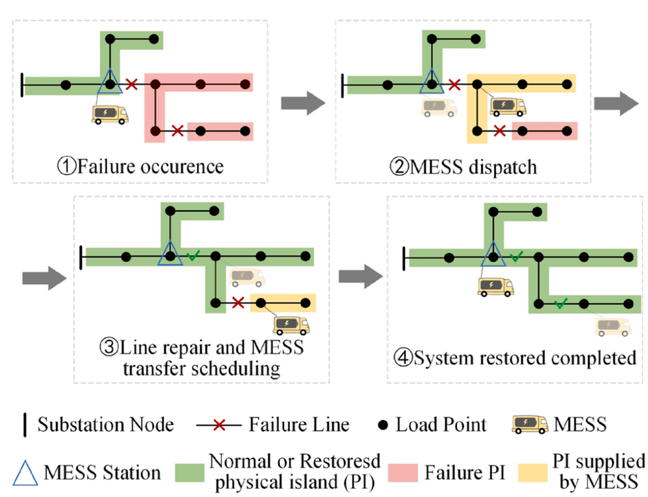

Fig. 1. MPS power supply strategy.

lower in the order of power supply according to the power supply strategy wait for the nodes ranked higher to restore normal power supply by repairing the faults. For the failure nodes with the highest priority power supply, the waiting time t_w is zero. The traffic time t_{ra} is the time it takes for the MPS to move from the previous power supply node to the current node, and is related to distance and traffic congestion which is calculated using the traffic impedance function proposed by U. S. Bureau of Public Roads as follows [33]:

$$t_{ra} = \widetilde{t}_{ra}\left[1 + \alpha_1 \left(\frac{q_\alpha}{C_\alpha}\right)^{\beta_1}\right] \tag{1}$$

where $\widetilde{t}_{ra}$ is the driving time of the MPS in the state of free prevailing driving, C_α is the capacity of road α, q_α is the traffic volume of road α, α_1 and β_1 are the retardation coefficients. The installation time t_i is the time required for the MPS to be installed to the corresponding node. Therefore, the outage time of a failure node using MPS backup power is calculated as follows [34,35]:

$$t_o = t_w + t_{ra} + t_i \tag{2}$$

2.2. Evaluation scenario

Based on the evaluation time scales and the magnitude of system failure risk, the evaluation scenarios are categorized into long-term reliability evaluation and short-term resilience evaluation. Reliability evaluation quantifies the system ability to continuously deliver qualified power to users under normal operating conditions. It primarily focuses on analyzing the system performance under random component failures, with particular attention to the frequency, duration, and extent of power interruptions. In contrast, resilience assessment evaluates the system ability to anticipate, resist, absorb, respond to, and recover from high-impact disturbances such as natural disasters or deliberate attacks. Reliability evaluation targets low-impact, high-probability random failures, while resilience evaluation addresses high-impact, low-probability extreme events. The reliability evaluation uses an annual time scale, reflecting the system ability to continuously supply power to users over long-term operation. The resilience evaluation, on the other hand, uses an hourly time scale, reflecting the system ability to maintain power supply to users in the short term under the impact of extreme events. In reliability evaluation, only random component failures are considered, with low component failure risk. The system experiences a single failure. When the failure component is repaired, all nodes return to normal power supply, and the MPS only needs to carry out one dispatch. In resilience evaluation, the risk of component failure increases due to extreme events, leading to multiple failures in the system. With limited repair resources, important components are prioritized for repair. Therefore, the MPS dispatch is coordinated with the repair process. As components are repaired, the number of failure nodes decreases, and the MPS makes dispatch decisions based on the evolving state of the failure nodes to maximize the system resilience. Additionally, the evaluation indices differ between the two evaluation scenarios. The evaluation indices for long-term reliability evaluation are based on failure rates, which are frequency-based indices, while the indices for short-term resilience evaluation are based on availability, which are probability-based indices.

3. Long-term reliability evaluation

This section introduces the long-term reliability evaluation method for distribution systems that include MPSs. First, the evaluation process is described, followed by reliability evaluation method for ordinary nodes, nodes with distributed generation (DG) backup power supply, and nodes with MPS backup power supply. Finally, system reliability indices and their calculation methods are presented.

3.1. Evaluation process

The process for long-term reliability evaluation of a distribution system with MPSs is shown in Fig. 2. First, the required data for evaluation is input, including network topology data, load data, DG data, and MPS data. Next, the reliability of each node is assessed using the minimal path set method, where the component set of the power supply paths for each node is determined, and the failure frequency of each node is calculated. After considering the dispatch of MPS in response to component failures, the consequences of failures at each node are analysed, and node reliability indices are calculated. Finally, based on the reliability indices of individual nodes, the overall system reliability indices are calculated, completing the reliability evaluation of the distribution system.

3.2. Node reliability evaluation

The purpose of node reliability evaluation is to evaluate the reliability level of power supply for individual nodes. The evaluation indices include annual failure rate λ_j^n, annual outage time U_j^n, annual average availability A_j^n, and annual expected energy not supplied $EENS_j^n$. The reliability level of a node is influenced by factors such as network topology, the failure risk of the power supply path, and the configuration of interconnection switch, DG, and MPS. Generally, nodes located upstream in the network have shorter power supply paths, lower failure risk, and higher reliability. Nodes equipped with interconnection switch, DG, or MPS can continue to receive power through alternative supply paths in the event of a failure in the primary supply path, resulting in higher reliability. The following subsections will introduce the method for calculating reliability indices for ordinary nodes, nodes with DG backup power supply and nodes with MPS backup power supply.

3.2.1. Ordinary node

In a distribution system, the ordinary node refers to the node supplied by a single path from the distribution substation. The reliability evaluation of ordinary nodes uses the minimal path set method [36], identifying the minimal cut sets for each node. The minimal cut set for an ordinary node consists of the components located on the power supply path upstream of the node, as well as the components downstream of the node before the circuit breaker. When these components fail, the node experiences a power outage until the failure component is repaired, after which the node regains power. Therefore, the annual failure rate λ_j^n of node j is calculated as follows:

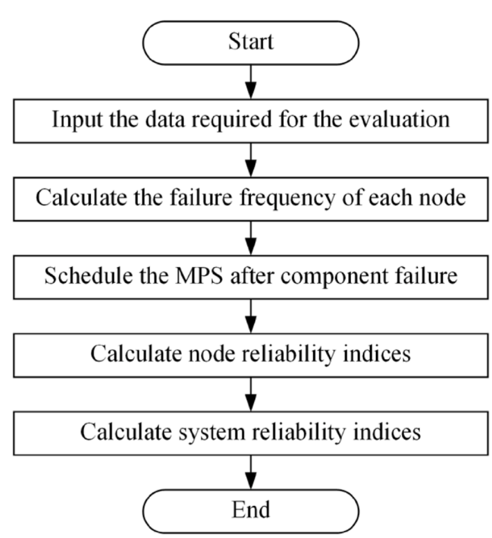

Fig. 2. Long-term reliability evaluation process.

$$\lambda_j^n = \sum_{i \in S_j} \lambda_i^c \tag{3}$$

where λ_i^c is the failure rate of component i, and S_j is the minimal cut set of node j.

The annual outage time U_j^n of node j is calculated as follows:

$$U_j^n = \sum_{i \in S_j} \lambda_i^c \cdot t_r \tag{4}$$

where t_r is the repair time of failure component.

The annual average availability A_j^n of node j is calculated as follows:

$$A_j^n = \frac{8760 - U_j^n}{8760} \cdot 100\% \tag{5}$$

The annual expected energy not supplied $EENS_j^n$ of node j is calculated as follows:

$$EENS_j^n = U_j^n \cdot L_j \tag{6}$$

where L_j is average load of node j.

3.2.2. Node with DG backup power supply

DG can serve as a backup power path for nodes, providing continued electricity supply when the main power path fails, thereby enhancing the reliability of the nodes. DG mainly includes diesel generators, wind turbine generators (WTG), photovoltaic (PV), and energy storage (ES). The output modeling for these types of DG is introduces as follows.

(1) Diesel Generator

The output of the diesel generator is determined by its operating state and rated power limits. The operating state is represented using a two-state Markov model [36]. If the diesel generator is in a normal operating state, it can provide output as needed within the rated power limits; if it is in a failure state, the output is zero. The calculation method for diesel generator output P_d is as follows [37]:

$$P_d = s_d \cdot P_d{}', 0 \le P_d{}' \le P_r^d \tag{7}$$

where s_d is the state of the diesel generators; $P_d{}'$ is the output of the diesel generator according to the load demand; P_r^d is the rated power of diesel generator.

(2) WTG

The output of WTG is determined by both its operational state and output characteristic curve. When the WTG experiences a fault, its output is zero. When the wind turbine is in normal operation, its output is determined by the wind speed. The output of WTG P_w is calculated as follows [38]:

$$P_w = \begin{cases} 0, v_w \le V_{ci} or v_w \ge V_{co} \\ s_w \cdot P_r^w \cdot (A + B \times v_w + C \times {v_w}^2), V_{ci} < v_w \le V_r \\ s_w \cdot P_r^w, V_r < v_w < V_{co} \end{cases} \tag{8}$$

where s_w is the state of the wind turbine; P_r^w is the rated power of wind turbine; v_w is the wind speed, V_{ci} is cut-in wind speed, V_r is rated wind speed, V_{co} is cut-out wind speed.A, B, C are polynomial fitting coefficients, which are calculated as follows:

$$\begin{aligned} A &= \left(V_{ci}(V_{ci} + V_r) - 4(V_{ci} \cdot V_r) \left(\frac{V_{ci} + V_r}{2V_r} \right)^3 \right) \Big/ (V_{ci} - V_r)^2 \\ B &= \left(4(V_{ci} + V_r) \left(\frac{V_{ci} + V_r}{2V_r} \right)^3 - (3V_{ci} + V_r) \right) \Big/ (V_{ci} - V_r)^2 \\ C &= \left(2 - 4 \left(\frac{V_{ci} + V_r}{2V_r} \right)^3 \right) \Big/ (V_{ci} - V_r)^2 \end{aligned} \tag{9}$$

(3) PV

The output of PV system is determined by operating state and output characteristic curve. Since the PV system consists of several PV units which operate independently of each other, the failure of one unit will not affect the normal operation of other units. Therefore, a derated operating state is introduced to describe the output of the PV system, as shown in Fig. 3 [39], where μ_{pvu} is the repair rate of the PV unit and λ_{pvu} is the failure rate of the PV unit. A PV system consisting of n PV units has $n + 1$ operating states. The calculation method for the output of PV system P_{pv} is as follows [40]:

$$P_{pv} = \sum_{i=1}^{n} s_i^{pv} \cdot r \cdot a_{pv} \cdot \eta \tag{10}$$

where s_i^{pv} represents the state of PV unit i; r is solar irradiance; a_{pv} is area of PV panel; η is conversion efficiency of PV units.

(4) ES

The ES system has four operating states: charging, discharging, float charge, and failure. In the charging state, the system charges the ES; once fully charged, the ES enters the float charge state, where the voltage and current are low and the power consumption can be ignored. In the discharging state, the ES acts as a power source; once depleted, it enters the outage state, which is simplified to be categorized as the failure state. In the charging, discharging and floating states, there is a possibility of failure and entering the failure state. The state transition process of the ES is shown in Figure 4. The calculation method for the output of the ES system P_e is as follows [37]:

$$P_e = \begin{cases} 0, failureorfloatchargingstate \\ P'_e, dischargingstate \\ -P_{e,c}, chargingstate \end{cases} \tag{11}$$

where P'_e is the output of the ES according to the load demand; $P_{e,c}$ is the charging power of the ES.

The integration of DG can enhance the reliability of the corresponding nodes. When the component on the main power path of the node fails, it can switch to the backup power path supplied by DG. The demand and amount of load shedding is based on the output and load of

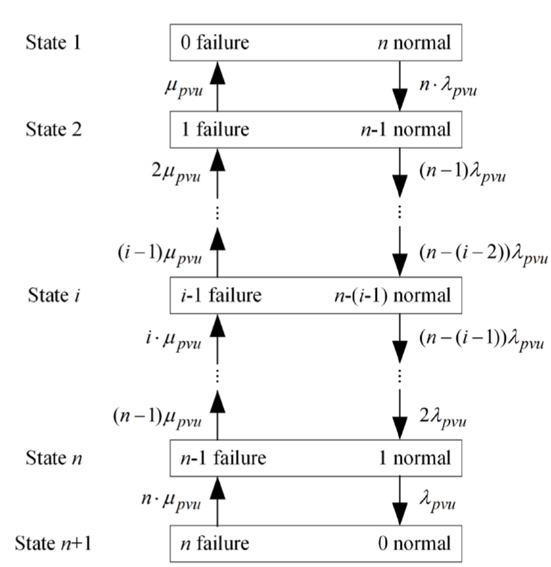

Fig. 3. State transition process of PV.

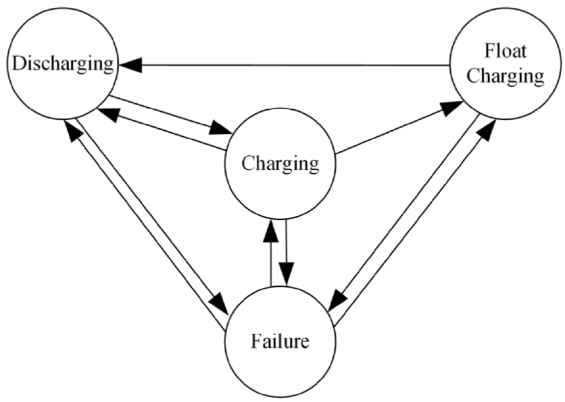

Fig. 4. State transition process of the ES.

the DG. Considering the switching time of the backup power path, the integration of DG does not affect frequency-related indices. The annual failure rate of the node is calculated using (3).

When the main power path of the node fails, if the backup power path also fails, the outage time for the node is equal to the repair time of the failure component. If the output of the diesel generator or renewable energy DG on the backup power path is less than the node load, the node will experience load shedding, resulting in the partial outage event. Conversely, if the output of the distributed generation on the backup power supply path exceeds the node load, the outage time for the node will be the switching time of the power path. The calculation method for the annual failure time of the node U_j^n with diesel generators or renewable energy DG on the backup power path is as follows:

$$U_j^n = \lambda_j^n \cdot \left(p_j^{af} \cdot t_r + \left(1 - p_j^{af}\right) \cdot \left(s_{lc} \cdot \left(P_{DG} \cdot t_s + \left(L_j - P_{DG}\right) \cdot t_r\right) / L_j + (1 - s_{lc}) \cdot t_s\right)\right) \tag{12}$$

where p_j^{af} is the failure probability of the backup power path; t_r is the repair time of failure component; s_{lc} represents the load shedding status of the node, where 1 indicates that the node sheds load and 0 indicates that the node does not shed load; P_{DG} is the output of DG; t_s is the switching time of the power path. When the node is not a DG installation node, P_{DG} becomes the remaining output after the distributed generation supplies the upstream nodes of the evaluation node.

If the ES is installed on the backup power path, it is assumed that it acts as a backup power source under normal operation and is in a fully charged state when a component on the main power path of the node fails. If the stored energy can supply power to the node until the failure component is repaired, no load shedding will occur; otherwise, the node will need to shed load. The failure time for the node is calculated as follows:

$$U_j^n = \lambda_j^n \cdot \left(p_j^{af} \cdot t_r + \left(1 - p_j^{af}\right) \cdot \left(s_{lc} \cdot \left(t_r - E_r / L_j\right) + (1 - s_{lc}) \cdot t_s\right)\right) \tag{13}$$

where E_r is the rated capacity of ES.

The annual average availability and the annual expected energy not supplied for nodes with backup power from distributed generation can be calculated using formulas (5) and (6).

3.2.3. Node with MPS backup power supply

In long-term reliability evaluation, the component failure rate is low, allowing the system to be considered as experiencing single failure. After a component failure, the dispatching of the MPS is based on the load size, importance of the outage node, and the power capacity of the MPS. If the load of the outage node exceeds the total power capacity of all MPSs, load shedding is required. If the load of the outage node does not exceed the total power capacity of all MPSs, no load shedding is required. Due to the travel and installation time required for MPS backup power, it does not affect the failure frequency of the node. The annual failure frequency of the node is calculated using (3). Since MPS is divided into MEG and MESS, and MESS has capacity limitations, it is necessary to differentiate between MEG and MESS power supply when calculating the annual outage time for nodes powered by MPS backup. The calculation method for the annual outage time of the node is as follows:

$$\begin{aligned} U_j^n = \lambda_j^{MEG} \cdot & \left(s_{lc} \cdot \left(P_{MEG} \cdot t_o + \left(L_j - P_{MEG}\right) \cdot t_r\right)\right. \\ & \left. / L_j + (1 - s_{lc}) \cdot t_o\right) + \lambda_j^{MESS} \cdot \left(s_{lc} \cdot \left(t_r - E_r^{MESS} / L_j\right) + (1 - s_{lc}) \cdot t_o\right) \end{aligned} \tag{14}$$

where λ_j^{MEG} is the failure frequency of node j powered by MEG backup after the failure, λ_j^{MESS} is the failure frequency of node j powered by MESS backup after the failure, P_{MEG} is the output of MEG, and E_r^{MESS} is the rated capacity of MESS.

3.3. System reliability evaluation

In the long-term reliability evaluation of the distribution system, the system evaluation is carried out by counting the reliability indices of each node, which reflects the reliability of overall system during long-term operation. The system reliability indices include system average interruption frequency index *SAIFI*, system average interruption duration index *SAIDI*, customer average interruption duration index *CAIDI*, expected energy not supplied *EENS*, and average system availability index *ASAI*. The calculation methods for each index are as follows:

$$SAIFI = \frac{\sum_{j \in O} \lambda_j^n \cdot N_j}{\sum_{j \in O} N_j} \tag{15}$$

$$SAIDI = \frac{\sum_{j \in O} U_j^n \cdot N_j}{\sum_{j \in O} N_j} \tag{16}$$

$$CAIDI = \frac{\sum_{j \in O} U_j^n \cdot N_j}{\sum_{j \in O} \lambda_j^n \cdot N_j} \tag{17}$$

$$ASAI = \frac{8760 \sum_{j \in O} N_j - \sum_{j \in O} U_j^n \cdot N_j}{8760 \sum_{j \in O} N_j} \tag{18}$$

$$EENS = \sum_{j \in O} EENS_j \tag{19}$$

where O is the set consisting of all nodes of the system and N_j is the number of users of node j.

4. Short-term resilience evaluation

This section introduces the short-term resilience evaluation method for distribution systems with MPS. First, the evaluation process is described, followed by the MPS pre-disaster deployment and transfer strategies. Next, the node resilience evaluation method is introduced, and finally, the system resilience indices and their calculation methods are provided.

4.1. Evaluation process

The short-term resilience evaluation process for a distribution system with MPS is illustrated in Fig. 5. First, the required data for evaluation is input, including network topology data, load data, DG data, MPS data, and component failure risk data under extreme events. Next, MPS pre-disaster deployment is performed based on node and zone importance

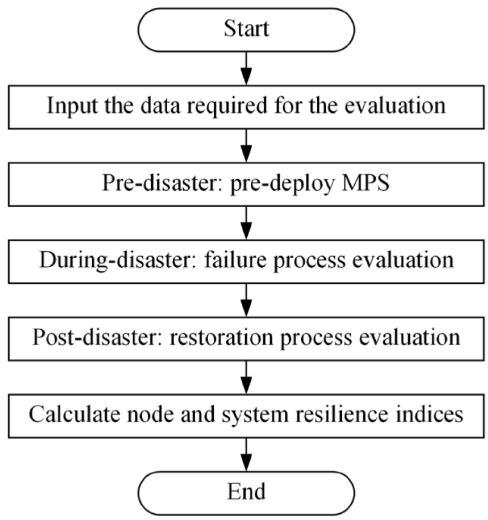

Fig. 5. Short-term resilience evaluation process.

and failure risk. Then, the system failure process during the extreme event is evaluated, assessing the instantaneous availability of nodes based on component failure risks under extreme events and network topology. Post-disaster, the restoration process is evaluated by considering the repair of failed components and MPS transfer strategies. Finally, resilience indices for nodes and the overall system are calculated, completing the short-term resilience evaluation of the distribution system under extreme events. In the evaluation, both load shedding and partial load restoration are considered. Due to the low voltage level and high capacity margin of distribution lines, capacity constraints are typically neglected, and node power availability is assessed based on network connectivity. Under extreme events, multiple component failures may occur. A node can be supplied if at least one of its supply paths remains normal; otherwise, it is considered to be in outage. Alternative supply paths may be available through interconnection switches or DGs. When the primary supply path fails, supply can be restored via switching operations, provided the backup path. For DG- or MPS-based restoration, both the condition of the supply path and the operational status of the DGs/MPSs must be considered. As DGs and MPSs are subject to power and capacity constraints, their dispatch strategies are determined based on network topology, switch configurations, and load priorities. Loads exceeding their supply limits result in unsupplied demand. During the restoration process, repair crews prioritize critical components to accelerate the recovery of load. As fault components are repaired, affected nodes regain power once their supply paths are restored. MPS units are dynamically reallocated based on repair progress to supply remaining nodes, with the amount of restored load constrained by their power and energy capacities.

4.2. MPS Pre-deployment and transfer strategies

For extreme events such as typhoons, floods, and ice storms, weather forecast information can be used pre-disaster to predict the intensity, duration, and impact range of the hazard. Based on these predictions, MPS can be pre-deployed to critical nodes and those with high failure risk before the disaster strikes, enhancing system resilience. Under extreme events, the importance of each node depends on its failure risk and the importance of the loads it supports. Therefore, the node importance index c_j^n is defined and calculated as follows:

$$c_j^n = \left(1 - A_j^n(t_d)\right) \cdot c_j^l \tag{20}$$

where $A_j^n(t_d)$ is the instantaneous availability of the node j at the time t_d when the extreme event ends, and c_j^l is the importance of the load connected to the node.

When the MPS output is sufficient, a single MPS can supply the power demands of multiple adjacent nodes. Based on MPS output, node load, and network topology, system nodes are partitioned into zones. The importance of a zone is determined by the sum of the importance values of all components within that zone. The zone importance c_h^z is then defined and calculated as follows:

$$c_h^z = \sum_{j \in Z_h} c_j^n \tag{21}$$

where Z_h is the set of nodes that make up zone h.

Based on the importance of each zone within the distribution system, MPS units are pre-deployed before the extreme event. Following component failures during the extreme event, MPS units rapidly supply power to the affected nodes, thereby enhancing system resilience. In the simulation method, each failure scenario is simulated through random sampling, and optimization is performed to minimize load loss, yielding both the repair strategy for failed components and MPS transfer strategy. However, in the analytical method, only the failure probabilities of components after a disaster are available, without any specific failure scenarios. As a result, it is not possible to directly apply optimization models to determine the allocation of MPSs and repair crews. Instead, the restoration strategies are developed based on probability theory, taking into account the expected failure risks and their potential impacts. Although the resulting strategies may not be strictly optimal when compared to those derived from scenario-based optimization, they are generally close to optimal in performance. This may lead to slightly conservative resilience evaluation results. Nevertheless, a key advantage of the analytical method lies in its ability to significantly improve evaluation efficiency by allowing a small and acceptable loss of accuracy. Since resilience evaluation is oriented toward practical engineering applications, such a minor deviation in accuracy is considered acceptable.

After the extreme event, the repair crews restore the failed components based on the component importance ranking. The importance of a component is related to its failure probability, its position in the network topology, the amount of load supplied by that component, the importance of the load, and the network topology. A component with a higher probability of failure is considered more critical. Generally, components located upstream of the line are more important. The importance of a component also increases with the number and importance of loads it supports. Moreover, the configuration of interconnection switches and DGs influences the component importance. The component importance index c_i^c is defined as the sum of the reductions in normal supply load due to component failures multiplied by the load importance. The calculation method is as follows:

$$c_i^c = \left(1 - A_i^c(t_d)\right) \cdot \left(\sum_{j \in SN_i} A_j^n(t_d) \cdot L_j \cdot c_j^l - \sum_{j \in SN_i} A_j^n(t_d) \Big|_{A_i^c(t_d)=0} \cdot L_j \cdot c_j^l \right) \tag{22}$$

where SN_i is the set of nodes that component i supplies, $A_j^n(t_d)|_{A_i^c(t_d)=0}$ is the instantaneous availability of node j assuming component i fails.

When the failed component on the current MPS service zone power path is repaired, the MPS will move to the next failure zone based on zone importance to power the affected nodes. The calculation formula for the improvement in the instantaneous availability of system nodes due to MPS transfer will be provided in the next subsection.

4.3. Node resilience evaluation

Under extreme events, the repair of failed components begins after the event has ended. Therefore, resilience evaluation for nodes and the system is divided into two processes: failure and restoration. In the resilience evaluation, hours are used as the time scale, and since this is a short-term evaluation, probability indices based on availability are used, rather than frequency-based indices common in reliability evaluations. Resilience evaluation employs the probability density evolution method [41], dividing the evaluation time into K time intervals, each with a duration of ΔT. This results in K+1 discrete time points:$T_0^f, T_1^f, T_2^f, \cdots, T_k^f, \cdots, T_K^f$.

$$A_i^c\left(T_k^f\right) = \exp\left\{-\int_0^{T_k^f} \lambda_i^c(t)dt\right\} \tag{23}$$

where $A_i^c(t)$ is the instantaneous availability of component i at time t; $\lambda_i^c(t)$ is the failure rate of component i at time t under the influence of the extreme event. In distribution system resilience evaluation, component failure rates are often derived from component vulnerability models combined with the intensity of extreme events. Typically, these vulnerability models are developed based on historical data using statistical fitting techniques or artificial intelligence approaches [29,42].

The instantaneous availability of a node is determined by the instantaneous availability of the components along its power supply path. For an ordinary node with only one power supply path, the calculation method for its instantaneous availability is as follows:

$$A_j^n\left(T_k^f\right) = \prod_{i \in S_j} A_i^c\left(T_k^f\right) \tag{24}$$

For nodes with DG as backup power supply path, the node can switch to the backup path for continued power supply if the main power supply path fails. The calculation method for the instantaneous availability of such a node is as follows:

$$A_j^n\left(T_k^f\right) = \prod_{i \in S_j} A_i^c\left(T_k^f\right) + \left(1 - \prod_{i \in S_j} A_i^c\left(T_k^f\right)\right) \cdot \prod_{i \in AS_j} A_i^c\left(T_k^f\right) \cdot A'_{DG}\left(T_k^f\right) \tag{25}$$

where AS_j is the set of components in the backup supply path and $A'_{DG}(t)$ is the equivalent availability of DG. The equivalent availability accounts for the uncertainty of renewable energy output and the capacity limitations of ES. The calculation method for the equivalent availability of renewable DGs such as WTG and PV is as follows:

$$A'_{DG}\left(T_k^f\right) = \begin{cases} A_{DG}\left(T_k^f\right), P_{DG}\left(T_k^f k\right) \geq L\left(T_k^f\right) \\ A_{DG}\left(T_k^f\right) \cdot \dfrac{P_{DG}\left(T_k^f\right)}{L\left(T_k^f\right)}, P_{DG}\left(T_k^f\right) < L\left(T_k^f\right) \end{cases} \tag{26}$$

where $P_{DG}(t)$ is the output of DG. When the evaluated node is not the installation site of DG, $P_{DG}(t)$ is the remaining output of DG after supplying the upstream nodes of the evaluated node.

The state of charge (SOC) of the MESS at each time step is iteratively calculated based on its SOC at the previous time step and the power supplied at each time. The calculation method is as follows:

$$E\left(T_k^f\right) = E\left(T_{k-1}^f\right) - P_{MESS}\left(T_{k-1}^f\right) \cdot \Delta t \tag{27}$$

Where $E\left(T_k^f\right)$ is the SOC of MESS at time T_{k-1}^f and $P_{MESS}\left(T_{k-1}^f\right)$ is output of the MESS at time T_{k-1}^f.

When there are overlapping components between the main supply path and the backup supply path, the instantaneous availability of the overlapping components in the backup supply path should be calculated using the conditional availability of the components under the assumption that the main supply path has failed. The calculation method is as follows:

$$\begin{aligned} \widehat{A}_i^c\left(T_k^f\right) &= \Pr\left\{s_i^c = 0 \middle| s_j^p = 1\right\} \\ &= \frac{\Pr\left\{s_j^p = 1 \middle| s_i^c = 0\right\} \cdot \Pr\{s_i^c = 0\}}{\Pr\left\{s_j^p = 1 \middle| s_i^c = 0\right\} \cdot \Pr\{s_i^c = 0\} + \Pr\left\{s_j^p = 1 \middle| s_i^c = 1\right\} \cdot \Pr\{s_i^c = 1\}} \\ &= \frac{\left(1 - \prod_{i' \in S_j, i' \neq i} A_{i'}^c\left(T_k^f\right)\right) \cdot A_i^c\left(T_k^f\right)}{\left(1 - \prod_{i' \in S_j, i' \neq i} A_{i'}^c\left(T_k^f\right)\right) \cdot A_i^c\left(T_k^f\right) + \left(1 - A_i^c\left(T_k^f\right)\right)} \end{aligned} \tag{28}$$

where $\widehat{A}_i^c(t)$ is the conditional instantaneous availability of the component i at time t; s_i^c denotes the state of the component i, in which 0 indicates normal operation and 1 indicates failure; s_j^p denotes the state of the power supply path for node j, in which 0 indicates normal operation and 1 indicates failure.

During the system failure process, repair crews cannot operate due to the extreme event, and as a result, MPS remain stationary. The calculation method for the instantaneous availability of nodes powered by MPS backup during the failure process is as follows:

$$A_j^n\left(T_k^f\right) = \prod_{i \in S_j} A_i^c\left(T_k^f\right) + \left(1 - \prod_{i \in S_j} A_i^c\left(T_k^f\right)\right) \cdot A'_{MPS}\left(T_k^f\right) \tag{29}$$

where $A'_{MPS}(t)$ is the equivalent availability of the MPS.

After the extreme event ends, the restoration process begins, with repair crews restoring failed components based on their importance. Similar to the failure process, a discrete time series $T_0^r, T_1^r, T_2^r, \cdots, T_k^r, \cdots, T_K^r$ is defined for the restoration process. At the start of the restoration process, the instantaneous availability of each component is equal to its availability at the end of the failure process.

If a component starts repair at time T_0^r, the probability that the repair time t_r falls within the interval $\left(T_{k-1}^r, T_k^r\right]$ is as follows:

$$\Pr\{T_{k-1} < t_r < T_k\} = G(T_{k-1}) - G(T_k) \tag{30}$$

where $G(t)$ is the repair time distribution function.

The repair sequence of components is determined based on their importance ranking. Assuming there are C repair teams, if the components ranked in the top C by importance fail, the expected start time of repair is the start time of the system restoration process T_0^r. At time T_0^r, for component i with low importance ranking, if the number of failed components that are more important than component i is less than C, then component i starts to be repaired at T_0^r. The probability is calculated as follows:

$$\begin{aligned} p_i^{rs}\left(T_0^r\right) &= \Pr\left\{F_i\left(T_0^r\right) < C\right\} \\ &= \sum\left(\prod_{i' \in IN_i}\left(\left(1 - s_{i'}^n\left(T_0^r\right)\right) \cdot A_{i'}^c\left(T_0^r\right) + s_{i'}^n\left(T_0^r\right) \cdot \left(1 - A_{i'}^c\left(T_0^r\right)\right)\right)\right)\Big|_{\sum s_{i'} < C} \end{aligned} \tag{31}$$

where $p_i^{rs}\left(T_0^r\right)$ is the probability that component $i$starts repair at T_0^r; $F_i\left(T_0^r\right)$ is the number of failure components with higher importance than component i; IN_i is the set of components with higher importance than component i; $s_{i'}^n\left(T_0^r\right)$ is the state of component i at T_0^r, where 0 indicates normal operation and 1 indicates failure.

If at time T_{k-1}^r, the number of failed components with higher importance than component i is greater than or equal to C, and at time T_k^r, the number of failed components with higher importance than component i becomes less than C, then component i starts to be repaired at time T_k^r. The probability is calculated as follows:

$$\begin{aligned} p_i^{rs}(T_k^r) &= \Pr\{F_i(T_{k-1}^r) \geq C \& F_i(T_k^r) < C\} \\ &= \sum \Big(\prod_{i' \in IN_i} \big((1 - s_{i'}^n(T_{k-1}^r)) \cdot A_{i'}^c(T_{k-1}^r) + s_{i'}^n(T_{k-1}^r) \cdot (1 - A_{i'}^c(T_{k-1}^r)) \cdot \\ & s_{i'}^n(T_k^r) \cdot (1 - A_{i'}^c(T_k^r)) + (1 - s_{i'}^n(T_k^r)) \cdot A_{i'}^c(T_k^r) \big) \Big) \Big|_{\sum s_{i'}^n(T_{k-1}^r) \geq C, \sum s_{i'}^n(T_k^r) < C} \end{aligned} \tag{32}$$

The instantaneous availability of a component at time T_k^r is equal to its instantaneous availability at the previous time T_{k-1}^r, plus the probability that the repair of the component was started at each of the previous times and completed at time T_k^r. The calculation method is as follows:

$$A_i^c(T_k^r) = A_i^c\left(T_{k-1}^r\right) + \left(1 - A_i^c\left(T_0^r\right)\right) \cdot \sum_{a=0}^{k-1} p_i^{rs}\left(T_a^r\right) \cdot \left(G\left(T_{k-a}^r\right) - G\left(T_{k-a-1}^r\right)\right) \tag{33}$$

As failed components are restored, when nodes in the zone where the MPS is located can be powered by the main supply path, the MPS will transfer to the next failure zone based on zone importance. If at timeT_{k-1}^r, the number of failed zones more important than zone h is greater than or equal to the number of MPS M, and at time T_k^r, the number of failed zones more important than zone h is less than M, then the MPS will start transferring at time $T_k^r$and begin providing backup power to zone h at time $T_k^r + t_{ra} + t_i$. The calculation method for this probability is as follows:

$$\begin{aligned} p_h^{ms}(T_k^r + t_{ra} + t_i) &= \Pr\{H_h(T_{k-1}^r) \geq M \& H_h(T_k^r) < M\} \\ &= \sum \Big(\prod_{i' \in IH_h} \big((1 - s_{h'}^z(T_{k-1}^r)) \cdot A_{h'}^z(T_{k-1}^r) + s_{h'}^z(T_{k-1}^r) \cdot (1 - A_{h'}^z(T_{k-1}^r)) \cdot \\ & s_{h'}^z(T_k^r) \cdot (1 - A_{h'}^z(T_k^r)) + (1 - s_{h'}^z(T_k^r)) \cdot A_{h'}^z(T_k^r) \big) \Big) \Big|_{\sum s_{h'}^z(T_{k-1}^r) \geq M, \sum s_{h'}^z(T_k^r) < M} \end{aligned} \tag{34}$$

where $p_h^{ms}(T_k^r + t_{ra} + t_i)$ is the probability that zone $h$starts MPS backup power supply at time $T_k^r + t_{ra} + t_i$; $H_h(T_k^r)$ is the number of failure zones in zones more important than zone h at time T_k^r;$s_{h'}^z(T_k^r)$ is the state of zone h at T_k^r, where 0 indicates normal operation and 1 indicates failure; $A_{h'}^z(T_k^r)$ is the instantaneous availability of zone h at T_k^r.

During the restoration process, the instantaneous availability of nodes is calculated using (24)-(29) based on the instantaneous availability of components. The calculation method for the instantaneous availability of nodes supplied by MPS transfer is as follows:

$$A_j^n(T_k^r) = \prod_{i \in S_j} A_i^c(T_k^r) + \left(1 - \prod_{i \in S_j} A_i^c(T_k^r)\right) \cdot A'_{MPS}(T_k^r) p_h^{ms}(T_k^r) \tag{35}$$

In short-term resilience evaluation, node indices are divided into two categories: instantaneous indices and average indices. Instantaneous indices reflect the damage state of a node at each moment during an extreme event, while average indices represent the overall damage state of the node throughout the event. Instantaneous node indices include instantaneous node availability $A_j^n(t)$, while average node indices include average availability $\widehat{A}_j^n$, expected outage time U_j^n, and expected energy not supplied $EENS_j$.

The instantaneous node availability is calculated using (23)-(35), and the method for calculating the average node availability is as follows:

$$\widehat{A}_j^n = \frac{\int_0^{t_e} A_j^n(t) dt}{t_e} \tag{36}$$

where t_e is the total evaluation time under the extreme event.

The expected outage time for node is calculated as follows:

$$U_j^n = \int_0^{t_e} \left(1 - A_j^n(t)\right) dt \tag{37}$$

The expected energy not supplied for node is calculated as follows:

$$EENS_j = \int_0^{t_e} \left(1 - A_j^n(t)\right) \cdot L_j(t) dt \tag{38}$$

4.4. System resilience evaluation

System resilience indices are categorized into instantaneous indices and average indices [29]. Instantaneous indices include system instantaneous availability $A_s(t)$ and instantaneous power not supplied $IPNS(t)$. Average indices include system average availability $\widehat{A}_s$ and system expected energy not supplied $EENS_s$.

The system instantaneous availability $A_s(t)$ is calculated as follows:

$$A_s(t) = \frac{\sum_{j \in O} A_j^n(t) \cdot N_j}{\sum_{j \in O} N_j} \tag{39}$$

The instantaneous power not supplied $IPNS(t)$ is calculated as follows:

$$IPNS(t) = \sum_{j \in O} \left(1 - A_j^n(t)\right) \cdot L_j(t) \tag{40}$$

The average system availability $\widehat{A}_s$ is calculated as follows:

$$\widehat{A}_s = \frac{\sum_{j \in O} \widehat{A}_j^n \cdot N_j}{\sum_{j \in O} N_j} \tag{41}$$

The system expected energy not supply $EENS_s$ is calculated as follows:

$$EENS_s = \sum_{j \in O} \left(\int_0^{t_e} \left(1 - A_j^n(t)\right) \cdot L_j(t) dt \right) \tag{42}$$

5. Numerical results

This section conducts long-term reliability evaluation and short-term resilience evaluation on the modified IEEE 123-node test system. The effectiveness and efficiency of the proposed method are validated by comparing the results with those obtained using the traditional simulation method. The calculations and simulations were performed using MATLAB R2023a on an Intel CORE i7-10700F PC with a clock speed of 2.9 GHz and 16 GB RAM.

5.1. The modified IEEE 123-node system

To validate the proposed method, an IEEE 123-node system was modified by incorporating MPS and specifying MPS station node. Additionally, four DGs were added, including a diesel generator, a WTG, a PV system, and an ES. The modified IEEE 123-node system consists of 123 nodes, 85 load nodes, 123 lines, 2 interconnection switches, and 4 DGs, as shown in Fig. 6. The supply areas of each DG are marked in yellow in the figure. The MPS resources consist of two MEGs and two MESSs. The main feeder zones and branch zones of the system are marked in green and blue areas, respectively. The topology, line, and node data of the IEEE 123-node system are obtained from reference [43]. The diesel generator has an output of 200 kW. The WTG is rated at 240 kW and has a cut-in wind speed of 3 m/s, a rated wind speed of 10 m/s and a cut-out wind speed of 25 m/s. The PV system is rated at 120 kW. The ES has a capacity of 500 kW with an output power of 140 kW and an input power of 40 kW. The MEG has a rated power of 200 kW and the MESS has a capacity of 250 kW with an output power of 150 kW. In

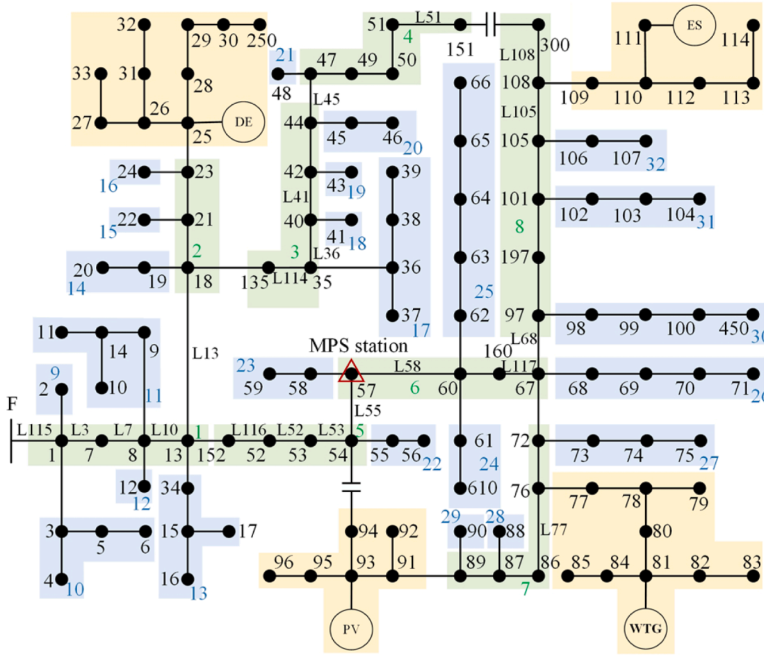

Fig. 6. Modified IEEE 123-node system.

the long-term reliability evaluation, the hourly wind speed data for the entire year was obtained by averaging the 30-year data (1991–2020) for the Washington area published by the U.S. National Centers for Environmental Information [44]. The hourly load profile and PV output ratio for the entire year were based on typical values provided in reference [45]. Under normal operating conditions, the failure rate of the lines is 0.065 failures per kilometer per year [21]. It is assumed that the repair time for failed lines follows a log-normal distribution with a mean of 5 hours [46,47]. In the short-term resilience evaluation, it is assumed that the extreme event is a wind storm. The failure risk of components is derived from their vulnerability curves under various wind speeds [48].

5.2. Long-term reliability evaluation

Considering the impact of MPS, the long-term reliability evaluation of the test system was performed using both the proposed analytical method and the traditional simulation method [21]. In the simulation method, a coefficient of variation less than 0.4 % was used as the convergence criterion. The system indices are shown in Table 1. The results obtained from the proposed analytical method and the simulation method differ by less than 0.5 %, demonstrating the accuracy of the proposed method. The calculation time for the proposed analytical method was 2.59 seconds, while the evaluation time for the simulation method was 3628 seconds, highlighting the efficiency of the proposed method.

Due to space limitations, the index results for a selection of nodes are provided in Table 2. Comparing the results obtained from the analytical method and the simulation method, the error for indices of node 1 is slightly larger than for other nodes. This is because node 1 is located upstream in the distribution system, where the reliability level is higher. For low-probability events, the simulation method requires a large number of scenarios to obtain accurate results. This also demonstrates the accuracy and superiority of the proposed analytical method. Node 28 and node 96 are nodes with DG backup power supply, with relatively high reliability levels. Node 28 is located near the DG installation node, while Node 96 is farther away, and its backup power is provided by a PV system, whose output is affected by weather conditions. Therefore, the reliability level of node 28 is higher than that of node 96. Node 49 and node 66 are nodes with MPS backup power supply. Although node 66 has a higher failure frequency than node 49, the reliability of node 66 is higher due to its proximity to the MPS station. The shorter time required for the MPS to move to node 66 for backup power contributes to its higher reliability compared to node 49. Fig. 7 presents the annual failure frequency and annual average availability results for all load nodes obtained using both the analytical method and the simulation method.

Table 1
The results of system indices of long-term reliability evaluation.

Index	Analytical Method	Simulation Method	error/%
SAIFI	0.2398	0.2409	0.4751
SAIDI/h	0.4107	0.4123	0.3982
CAIDI/h	1.7128	1.7115	0.0773
ASAI/%	99.9953	99.9952	1.87E-05
$EENS_s$/MW·h	1.4332	1.4389	0.3982
Calculation time/s	2.59	3628	/

Table 2
The results of node indices of long-term reliability evaluation.

Node	Index	Analytical Method	Simulation Method	error/%
1	λ_1^n	0.0260	0.025734	1.0334
	U_1^n/h	0.0476	0.047122	1.0334
	A_1^n/%	99.9995	99.9995	5.56E-06
	$EENS_1^n$/kW·h	1.9043	1.8848	1.0334
28	λ_{28}^n	0.1982	0.1987	0.2172
	U_{28}^n/h	0.0684	0.0685	0.2172
	A_{28}^n/%	99.9992	99.9992	1.7E-06
	$EENS_{28}^n$/kW·h	2.7358	2.7418	0.2172
49	λ_{49}^n	0.2340	0.23427	0.1154
	U_{49}^n/h	0.6670	0.6678	0.1154
	A_{49}^n/%	99.9924	99.9924	8.8E-06
	$EENS_{49}^n$/kW·h	93.3838	93.4917	0.1154
66	λ_{66}^n	0.2957	0.2977	0.6648
	U_{66}^n/h	0.4209	0.4237	0.6648
	A_{66}^n/%	99.9952	99.9952	3.22E-05
	$EENS_{66}^n$/kW·h	31.5711	31.7825	0.6648
96	λ_{96}^n	0.4046	0.4064	0.4440
	U_{96}^n/h	1.8501	1.8557	0.3025
	A_{96}^n/%	99.9789	99.9788	6.41E-05
	$EENS_{96}^n$/kW·h	37.0027	37.1150	0.3025

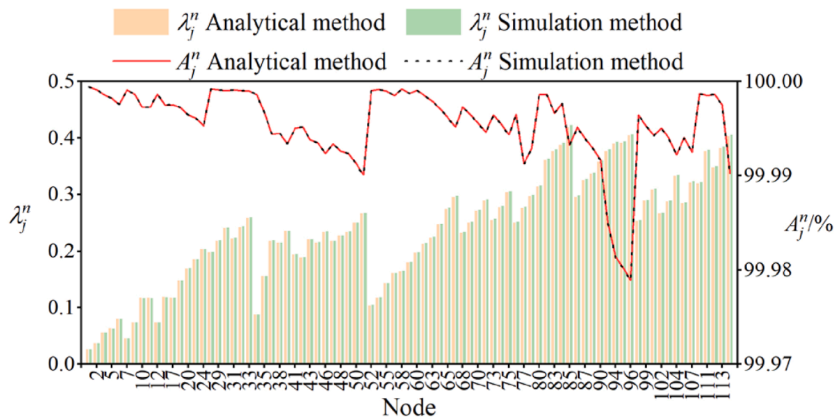

Fig. 7. Node failure frequency and availability in long-term reliability evaluation.

The consistency between the results of the two methods demonstrates the effectiveness of the proposed method. Comparative analysis of the reliability indices for different nodes helps identify weak nodes in the system, providing valuable guidance for improving the overall reliability level of the distribution system.

To investigate the impact of MPS and DG on the long-term reliability of the distribution system, four evaluation cases are listed in Table 3, and the long-term system reliability results under these cases are presented in Table 4. Comparing the four cases, the *SAIFI* remains consistent across all cases. However, with the inclusion of MPSs and DGs, the failure duration of nodes is reduced, leading to the higher reliability in the distribution system. The reliability in case 3 is higher than in case 2, owing to the flexibility of MPS, which allows it to provide backup power to a broader range of nodes during failure. It is important to note that the effectiveness of MPS and DG in improving system reliability is also influenced by their quantity and rated power. Conversely, the system exhibits the lowest reliability when neither MPS nor DG is deployed.

The availability of selected nodes under different cases is shown in Fig. 8. Node 1, located upstream in the distribution system with a short supply path and low failure rate, exhibits high reliability. After configuring MPS, the reliability of node 1 improves slightly. Nodes 28 and 96 are nodes with DG backup power supply. With DG considered, the reliability of these nodes improves. Node 28, powered by a diesel generator and located close to the DG installation site, exhibits higher reliability and greater improvement compared to node 96, which relies on PV backup power and is not adjacent to the PV installation site. Nodes 49 and 66 are supplied by MPS as backup. Without considering MPS, node 66 has a lower reliability level than node 49. However, when MPS is included, the reliability of node 66 improves more significantly due to its closer proximity to the MPS station, resulting in a higher reliability level than node 49.

Table 4
System reliability indices in different cases.

Index	Case 1	Case 2	Case 3	Case 4
SAIFI	0.2398	0.2398	0.2398	0.2398
SAIDI/h	0.4107	0.9735	0.6360	1.1988
CAIDI/h	1.7128	4.0601	2.6527	5
ASAI/%	99.9953	99.9889	99.9927	99.9863
$EENS_s$/MW·h	1.4332	3.3974	2.2197	4.1839

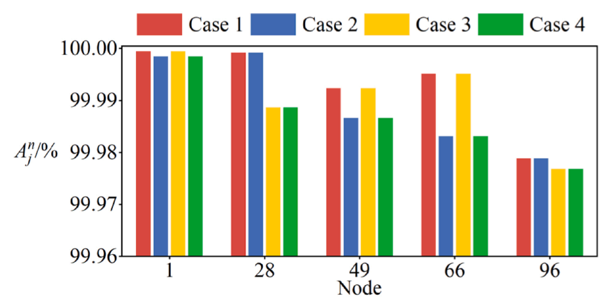

Fig. 8. Node availability in different cases.

5.3. Short-term resilience evaluation

The case study uses a storm as the extreme event. The wind speed, PV output proportion, and load proportion for the next 60 hours are shown in Fig. 9(b). It is assumed that MPS is pre-deployed before the storm. During the storm (0–24 hours), no repairs are conducted. After the storm ends, there is a 6-hour response waiting period before the repair process begins. The instantaneous system availability is shown in Fig. 9(a). Starting from the 10th hour, as wind speed increases, the instantaneous system availability rapidly decreases. At the 14th hour, when wind speed peaks, the rate of decline in instantaneous system availability reaches its maximum. Subsequently, as the wind speed decreases, the decline rate of the instantaneous system availability slows. By the 24th

Table 3
Evaluation cases.

Case	Evaluation Scenario
Case 1	Both MPSs and DGs are considered
Case 2	MPSs are not considered, DGs are considered
Case 3	MPSs are considered, DGs are not considered
Case 4	Neither MPSs nor DGs are considered

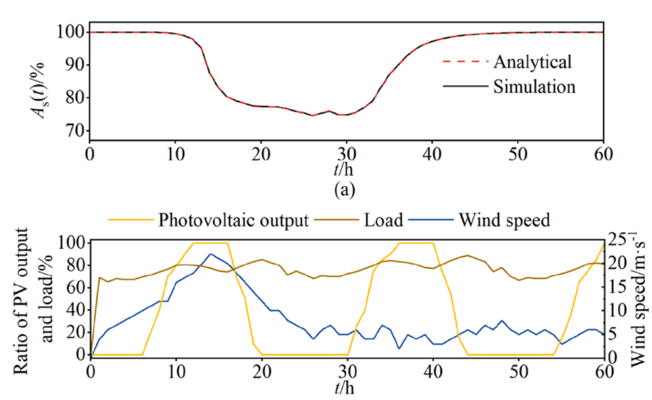

Fig. 9. Instantaneous system index of short-term resilience evaluation.

Table 5
The results of average system indices of short-term resilience evaluation.

Index	Analytical Method	Simulation Method	Error/%
$\widehat{A}_s$/%	91.5875	91.6425	0.0560
$EENS_s$/MW·h	18.2014	18.0840	0.6496
Calculation time/s	210	12750	/

hour, the instantaneous system availability drops to 76.7 %. During the 25th to 30th hour of the system response, the instantaneous system availability no longer remains constant, unlike the classical resilience trapezoidal curve. Instead, it fluctuates based on the output variations of renewable DGs. At the 30th hour, the restoration process begins, and as failure components are gradually repaired, the instantaneous system availability steadily improves. Simultaneously, the MPS is deployed to different zones. and by the 53rd hour, the instantaneous system availability reaches 99.9 %, marking the end of the storm's impact on the grid. The instantaneous availability curves obtained from the analytical method and the simulation method show a high degree of overlap, demonstrating the validity of the proposed method. In the recovery process, the instantaneous system availability obtained by the simulation method is slightly larger than that obtained by the analytical method, which is because the simulation method optimizes each failure scenario, and the repair strategy and MPS transfer strategy are optimal. In contrast, there is no specific failure scenario in the analytical method, and the repair strategy and MPS transfer strategy are proposed based on the probability expectation, which leads to a conservative evaluation result, but the evaluation error is small, while greatly improving the evaluation efficiency. The system average indices are presented in Table 5. The deviation from the results obtained using the simulation method is within 0.1 %, indicating the validity of the proposed method. The computation time of the proposed method is 210 seconds, compared to 12750 seconds for the simulation method, highlighting the efficiency of the proposed approach in short-term resilience evaluations.

Fig. 10 presents the top 20 critical lines ranked by importance, with their locations marked in Fig. 6. The importance of a line is influenced by its failure risk, the distribution system structure, its position within the system, and the load it supplies. Generally, lines with higher failure risks, those closer to the upstream of the system, or those supplying larger loads are more critical. In the short-term resilience evaluation proposed in this paper, restoration resources are allocated to components in descending order of importance during the restoration process. Furthermore, identifying critical components through importance ranking helps prioritize reinforcement measures, thereby enhancing the system resilience.

Fig. 11 illustrates the importance ranking of zones. The importance of a zone is determined by the failure risk of nodes within the zone and the loads connected to those nodes. Zones with higher node failure risks and larger connected loads have higher importance rankings. The pre-deployment of MPS resources is guided by the importance ranking of zones. In this case study, four MPS units are pre-deployed in zones 25, 4, 7, and 21 based on their importance. During the restoration process, as the repair crews fix failure components and these zones resume normal

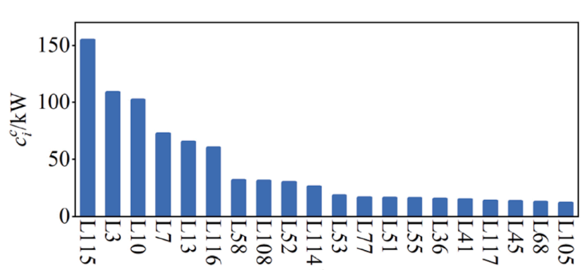

Fig. 10. Component importance ranking.

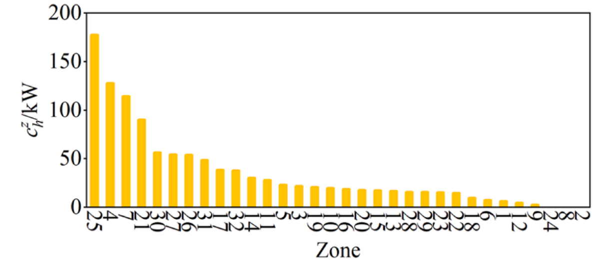

Fig. 11. Zone importance ranking.

Table 6
Average system resilience indices in different cases.

Index	Case 1	Case 2	Case 3	Case 4
$\widehat{A}_s$/%	91.58755	86.08674	89.87728	84.37795
$EENS_s$/MW·h	18.2014	30.1021	21.9019	33.7994

power supply, the MPS are relocated according to the importance rankings of other zones until the entire system is fully restored.

To investigate the impact of MPS and DG on the system resilience under extreme events, the test system was evaluated under the four cases presented in Table 4. The average system resilience indices are shown in Table 6. The case considering both MPS and DG achieves the highest system resilience. The resilience in the case considering only MPS is higher than that in the case considering only DG. In the case without MPS and DG, the system resilience is the lowest. The instantaneous system availability indices under the four cases are shown in Figure 12. When DG with renewable energy is considered, the system resilience curve during the response stage is no longer linear due to the variability of renewable energy output with environmental changes. A comparison of the four curves demonstrates that MPS and DG can enhance the system resilience under extreme events.

To verify the applicability of the proposed method to large-scale systems, we conducted long-term reliability and short-term resilience evaluations on a real 1,444-node distribution system from an urban area in southern China using different methods. The evaluation times are presented in Table 7. As the system scale increases, traditional analytical methods encounter the problem of dimensional explosion, significantly

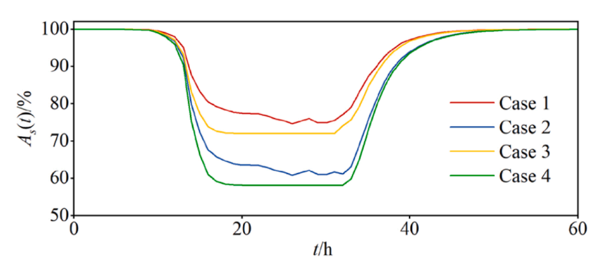

Fig. 12. Instantaneous system availability in different cases.

Table 7
Comparison of evaluation efficiency for different methods.

Method	IEEE 123-Node system		1444-Node real system	
	Reliability Evaluation	Resilience Evaluation	Reliability Evaluation	Resilience Evaluation
Proposed method	2.59s	210s	43s	3409s
Simulation method	3628s	12750s	46239s	383472s
Importance sampling simulation method	1076s	3108s	15767s	128325s

reducing computational efficiency. This is because traditional analytical methods use exhaustive enumeration to analyse system states from the component perspective. Specifically, by considering all possible states of each component to evaluate system reliability, if a component has two states—normal operation and failure—then a system with n components have 2^n states, leading to dimensional explosion. In contrast, the analytical method proposed in this paper does not analyse the system from the component perspective but rather from the node perspective. By determining the power supply path of a node, the node availability can be calculated using only the availability of components along its power supply path, thereby avoiding the dimensional explosion issue. Additionally, when calculating conditional availability and node availability, only basic arithmetic operations such as addition, subtraction, multiplication, and division are involved, without requiring advanced operations such as calculus or convolution. This significantly reduces computational demand, making it highly efficient for modern computers.

6. Conclusion

This paper presents an analytical approach for reliability and resilience evaluation of distribution systems with MPS, based on probabilistic expectation and the probability density evolution method. The proposed method offers advantages in terms of modeling concept, evaluation efficiency, and computational accuracy. Specifically, the paper first models MPS and divides the evaluation into long-term reliability evaluation and short-term resilience evaluation according to the evaluation timescale and the severity of system failure risks. Backup power supply strategies of MPS for failure nodes are proposed for both evaluations. Reliability and resilience evaluation methods are developed using probabilistic expectation and the probability density evolution method, along with evaluation indices. Finally, the method is validated on the modified IEEE 123-node system, achieving comparable accuracy to simulation methods, with less than 0.5 % error in reliability and less than 0.1 % error in resilience evaluation, while reducing computation time by approximately 1400 times and 60 times, respectively.

The proposed analytical method does not account for the impact of extreme events on the transportation network, nor does it incorporate coordinated dispatch strategies between MPSs and repair crews. In addition, the role of demand response is not considered in the current evaluation framework. Future research should aim to integrate these critical factors into reliability and resilience evaluation, which would enhance the practicality and accuracy of the evaluation.

CRediT authorship contribution statement

Gengfeng Li: Validation, Supervision, Resources, Project administration, Funding acquisition. **Dingmao Zhang:** Writing – review & editing, Writing – original draft, Visualization, Software, Methodology, Investigation, Formal analysis, Data curation, Conceptualization. **Zhaohong Bie:** Supervision, Investigation, Funding acquisition.

Declaration of competing interest

The authors declare that they have no known competing financial interests or personal relationships that could have appeared to influence the work reported in this paper.

Acknowledgements

This work was supported by the National Outstanding Youth Science Fund Project of National Natural Science Foundation of China (52222705).

Data availability

Data will be made available on request.

References

[1] Billinton R, Allan RN. Reliability evaluation of power systems. New York: Plenum Press; 1996.

[2] Furman J. Economic benefits of increasing grid resilience to weather outages. Tech. Rep. U.S. Dept. Energy; Aug. 2013. Online]. Available: https://www.energy.gov/sites/default/files/2013/08/f2/Grid%20Resiliency%20Report_FINAL.pdf.

[3] Salman AM, Li Y, Stewart MG. Evaluating system reliability and targeted hardening strategies of power distribution systems subjected to hurricanes. Reliab Eng Syst Saf 2015;144:319–33.

[4] Poudyal A, Poudel S, Dubey A. Risk-based active distribution system planning for resilience against extreme weather events. IEEE Trans Sustain Energy 2023;14:1178–92.

[5] Chen MR, Zeng GQ, Lu KD. Constrained multi-objective population xtremal optimization based economic-emission dispatch incorporating renewable energy resources. Renew. Energy 2019;143:277–94.

[6] Zeng GQ, Qin Z, Lu KD, Li LM. CMOPEO-OP: constrained multi-objective population extremal optimization-based optimal planning of standalone microgrids. Swarm Evol Comput 2024;92:101787.

[7] Xie HP, Tang LF, Zhu H, Cheng XF, Bie ZH. Robustness assessment and enhancement of deep reinforcement learning-enabled load restoration for distribution systems. Reliab Eng Syst Saf 2023;237:109340.

[8] Zhang C, Li YF, Zhang HX, Wang YJ, Huang YL, Xu JY. Distributionally robust resilience optimization of post-disaster power system considering multiple uncertainties. Reliab Eng Syst Saf 2024;251:110367.

[9] Tian M, Zhu ZY, Dong ZC, Zhao L, Yao HT. Resilience enhancement of cyber–physical distribution systems via mobile power sources and unmanned aerial vehicles. Reliab Eng Syst Saf 2025;254:110603.

[10] Wang W, He YF, Wang HB, Chen HZ, Xiong XF. Improving interdependent urban power and gas distribution systems resilience through optimal scheduling of mobile emergency supply and repair resources. Reliab Eng Syst Saf 2024;250:110303.

[11] Zhang ZJ, Dehghanian P, Nazemi M. Seismic-resilient electric power distribution systems: harnessing the mobility of power sources. IEEE Trans Ind Appl 2020;56:2304–13.

[12] Wang W, Xiong XF, He YF, Hu J, Chen HZ. Scheduling of separable mobile energy storage systems with mobile generators and fuel tankers to boost distribution system resilience. IEEE Trans Smart Grid 2022;13:443–57.

[13] Wang HP, Fang YP, Zio E. Resilience-oriented optimal post-disruption reconfiguration for coupled traffic-power systems. Reliab Eng Syst Saf 2022;222:108408.

[14] Hussain A, Bui VH, Kim HM. Optimal sizing of battery energy storage system in a fast EV charging station considering power outages. IEEE Trans Transp Electrific 2020;6:453–63.

[15] Jin YW, Acquah MA, Seo M, Han S. Optimal siting and sizing of EV charging station using stochastic power flow analysis for voltage stability. IEEE Trans Transp Electrific 2024;10:777–94.

[16] Lei SB, Chen C, Hou YH. Routing and scheduling of mobile power sources for distribution system resilience enhancement. IEEE Smart Grid 2019;10:5650–62.

[17] Wang SY, Bo R. resilience-oriented multi-stage adaptive distribution system planning considering multiple extreme weather events. IEEE Trans Sustain Energy 2023;14:1193–204.

[18] Lei SB, Chen C, Li YP, Hou YH. Resilient disaster recovery logistics of distribution systems: co-optimize service restoration with repair crew and mobile power source dispatch. IEEE Trans Smart Grid 2019;10:6187–202.

[19] Wang Y, Qiu DW, Teng F, Strbac G. Towards microgrid resilience enhancement via mobile power sources and repair crews: a multi-agent reinforcement learning approach. IEEE Trans Power Syst 2024;39:1329–45.

[20] Li JQ, Xu XY, Yan Z, Wang H, Shahidehpour M, Xie BP. Resilient resource allocations for multi-stage transportation-power distribution system operations in hurricanes. IEEE Trans Smart Grid 2024;15:3994–4009.

[21] Billinton R, Li WY. Reliability assessment of electric power systems using Monte Carlo methods. New York: Plenum Press; 1996.

[22] Hou G, Muraleetharan KK, Panchalogaranjan V, Moses P, Javid A, Al-Dakheeli H, et al. Resilience assessment and enhancement evaluation of power distribution systems subjected to ice storms. Reliab Eng Syst Saf 2023;230:108964.

[23] de Quevedo PM, Contreras J, Mazza A, Chicco G, Porumb R. Reliability assessment of microgrids with local and mobile generation, time-dependent profiles, and intraday reconfiguration. IEEE Trans Ind Appl 2018;54:61–72.

[24] Xu NZ, Chun CY. Reliability evaluation of distribution systems including vehicle-to-home and vehicle-to-grid. IEEE Trans Power Syst 2016;31:759–68.

[25] Mishra DK, Ghadi MJ, Li L, Zhang JF, Hossain MJ. Active distribution system resilience quantification and enhancement through multi-microgrid and mobile energy storage. Appl Energy 2022:118665.

[26] Muñoz-Delgado G, Contreras J, Arroyo JM. Reliability assessment for distribution optimization models: A non-simulation-based linear programming approach. IEEE Trans Smart Grid 2018;9:3048–59.

[27] Tabares A, Muñoz-Delgado G, Franco JF, Arroyo JM, Contreras J. An enhanced algebraic approach for the analytical reliability assessment of distribution systems. IEEE Trans Power Syst 2019;34:2870–9.

[28] Arefi A, Ledwich G, Nourbakhsh G, Behi B. A fast adequacy analysis for radial distribution networks considering reconfiguration and DGs. IEEE Trans Smart Grid 2020;11:3896–909.
[29] Zhang DM, Li GF, Bie ZH. An analytical method for resilience evaluation of distribution system based on instantaneous availability increment and probability density evolution. IEEE Trans Power Syst 2025:1–13.
[30] Chen YY, Zheng Y, Luo FJ, Wen JH, Xu Z. Reliability evaluation of distribution systems with mobile energy storage systems. IET Renew Power Gener 2016;10: 1562–9.
[31] Bajpai P, Chanda S, Srivastava AK. A novel metric to quantify and enable resilient distribution system using graph theory and Choquet integral. IEEE Trans Smart Grid 2018;9:2918–29.
[32] Zhang G, Zhang F, Wang XY, Zhang X. Fast resilience assessment of distribution systems with a non-simulation-based method. IEEE Trans Power Del 2022;37: 1088–99.
[33] Chen Z, Zheng C, Tao T, Wang Y. Reliability analysis of urban road traffic network under targeted attack strategies considering traffic congestion diffusion. Reliab Eng Syst Saf 2024;248:110171.
[34] Liu N, Hu XJ, Ma L, Yu XH. Vulnerability assessment for coupled network consisting of power grid and EV traffic network. IEEE Trans Smart Grid 2022;13: 589–98.
[35] Wang QY, Zhou W, Lv LE. Theory and application study of the road traffic impedance function. J Highway Transp Res Develop 2004;9:82–5.
[36] Li GF, Huang YX, Bie ZH. Reliability evaluation of smart distribution systems considering load rebound characteristics. IEEE Trans Power Syst 2018;9:1713–21.
[37] Li GF, Zhang DM, Sun SH, Bie ZH. Reliability evaluation method for power distribution systems with renewable distributed generations and adjustable loads. IET Gener Transm Distrib 2025;19:1–11.
[38] Ding Y, Wang P, Goel L, Loh PC, Wu QW. Long-term reserve expansion of power systems with high wind power penetration using universal generating function methods. IEEE Trans Power Syst 2011;26:766–74.
[39] Karngala AK, Singh C. Impact of system parameters and geospatial variables on the reliability of residential systems with PV and energy storage. Appl Energy 2023; 344:121266.
[40] Moharil RM, Kulkarni P S. Reliability analysis of solar photovoltaic system using hourly mean solar radiation data. Solar Energy 2010;84:691–702.
[41] Zhang DM, Li GF, Bie ZH, Fan KJ. An analytical method for reliability evaluation of power distribution system with time-varying failure rates. Reliab Eng Syst Saf 2024;250:110290.
[42] Li GF, Huang GC, Bie ZH, Huang YX. Component importance assessment of power systems for improving resilience under wind storms. J Modern Power Syst Cleanm Energy 2019;7:676–87.
[43] Kersting WH. Radial distribution test feeders. IEEE Trans Power Syst 1991;6: 975–85.
[44] NOAA National Centers for Environmental Information. Hourly/sub-Hourly observational data. https://www.ncei.noaa.gov/maps/hourly/; 2024.
[45] Alam MN, Chakrabarti S, Liang XD. A benchmark test system for networked microgrids. IEEE Trans Ind Inf 2020;16:6217–30.
[46] Arif A, Ma SS, Wang ZY, Wang JH. Optimizing service restoration in distribution systems with uncertain repair time and demand. IEEE Trans Smart Grid 2018;33: 6828–38.
[47] Fogliatto M, Caetano H, N LD, Massignan J, Fanucchi R, London J, et al. Power distribution system interruption duration model using reliability analysis regression. Electr Power Syst Res 2022;211:108193.
[48] Alvehag K, Söder L. A reliability model for distribution systems incorporating seasonal variations in severe weather. IEEE Trans Power Del 2011;26:910–9.